JOURNAL OF SOLID STATE CHEMISTRY 112, 120–125 (1994)

Copper Extraction from $TlCu_3S_2$—A Neutron Diffraction and Electronic Structure Calculation Study

R. Berger,* R. Dronskowski,† and L. Norén*

*Institute of Chemistry, Uppsala University, P.O. Box 531, S-751 21 Uppsala, Sweden; and †Max Planck Institute for Solid State Research, Heisenbergstrasse 1, D-70 569 Stuttgart, Germany

Received November 22, 1993; in revised form March 30, 1994; accepted April 4, 1994

The mechanism of the $TlCu_3S_2/TlCu_2S_2$ phase transformation has been studied experimentally by neutron diffraction and theoretically by three-dimensional extended Hückel band calculations. Experiments show that only one of the sites is attacked during the oxidative extraction of copper from $TlCu_3S_2$, the site that according to the calculations should be the most vulnerable. The results support a previously presented transformation mechanism model based on topotaxy.

INTRODUCTION

Previous experiments have shown that copper may be extracted from many phases in the Tl–Cu–S and Tl–Cu–Se systems. Chemical oxidation techniques have been used, with air as oxidant for the selenides (1, 2) or *in situ* formed oxygen (through hydrogen peroxide decomposition) for the sulfides (3). Electrochemistry also allows the reverse process, as was demonstrated for $TlCu_3Se_2/TlCu_2Se_2$ (4) and $TlCu_3Se_2/TlCu_2S_2$ (5). A similar couple was found in KCu_5S_3/KCu_4S_3 (6). In all these cases, the phase with less copper is a metal, as demonstrated by resistivity measurements on $TlCu_2Se_2$ (7, 8), $TlCu_2S_2$ (3), and KCu_4S_3 (9). The metallic properties are due to the presence of one valence-band hole per formula unit as directly measured from the Hall effect (3, 8, 9) or indirectly supported by chemical substitution (10).

There is less evidence that copper deficiency will lead to metallic behavior in the phases that normally are semiconducting if stoichiometric. For instance, a slight deviation from strict stoichiometry of $TlCu_5Se_3$ (11) leads to a linear temperature dependence of the Seebeck coefficient. Moreover, its positive value and small positive slope indicate that valence-band holes occur. Likewise, the mineral *crookesite*, which is copper-deficient $TlCu_7Se_4$, is a metallic conductor (12) and its Seebeck coefficient indicates that increasing copper deficiency is accompanied by the formation of valence-band holes (1).

It is likely that copper deficiency is always followed by valence-band holes not only in the structural series $TlCu_{2n}S_{n+1}$ (2), but in all cases where a formal charge picture of Tl(+), Cu(+), and S/Se(−2) will not do. Various X-ray photoelectron spectroscopy (XPS) measurements (9, 13) have shown that copper is invariably monovalent in its heavier chalcogenides. Hence, a deviation in stoichiometry does not evoke any mixed valence copper but rather holes in the top of the valence band.

In this study we wanted to test a model advocated previously (2) for the $TlCu_3X_2/TlCu_2X_2$ (X = S, Se) transformations. It was suggested that copper extraction from $TlCu_3X_2$ occurs preferentially within certain copper-rich slabs discerned in the structure and that a 50% copper depletion here followed by crystal shear would yield the final stoichiometry and structure. Some microstructural support (viz., oriented parallel cracks of a polished surface) was gained in the previous $TlCu_3Se_2/TlCu_2Se_2$ study (4). To obtain more details, we now used two approaches: one experimental, in which we investigated the progress of copper deficiency in $TlCu_3S_2$ (on the three crystallographic sites) by diffraction; and one theoretical, in which we sought evidence for weaker Cu–S bonding on any of these sites. In this paper we report our findings, which in fact give further support to the topotactic model (2).

THE STRUCTURES OF $TlCu_3X_2$ AND $TlCu_2X_2$ AND THE TRANSFORMATION MODEL

The structures of $TlCu_3X_2$ and $TlCu_2X_2$ (X = S, Se) are given in Fig. 1. In these projections a common slab with the composition $TlCu_2X_2$ has been accentuated to show the resemblance between the monoclinic $CsAg_3S_2$ on the one hand and the $ThCr_2Si_2$ structure type on the other. With this kind of representation (2), the former is built of two types of slabs, **A** and **B**, that alternate (sequence |**ABAB**|), while the latter contains only **A** slabs. This crystal-chemical view also connects the $Rb_3Cu_8S_6$ (14) (sequence |**ABA**|) and $Tl_5Cu_{14}S_{10}$ (15) (sequence |**ABABA**|) structures to the same theme.

The transformation of $TlCu_3X_2$ into $TlCu_2X_2$ involves a formal sequence change |**ABAB**. . .| → |**AAAA**. . .|,

0022-4596/94 $6.00

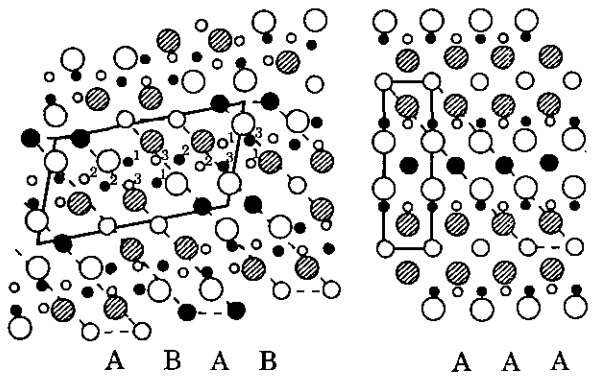

FIG. 1. Projections on (010) of monoclinic $TlCu_3X_2$ (*left*) and tetragonal $TlCu_2X_2$ (*right*). Large circles, sulfur or selenium; medium circles, thallium; small circles, copper. The atoms are situated at $y = 0$ (unfilled) or $y = \frac{1}{2}$ (filled or hatched). The conventional unit cells are given with solid lines. The common *monoclinic* $TlCu_2X_2$ building block (forming **A** slabs; see text) has been accentuated by dashed lines. The figures denote the different copper sites given explicitely in Table 1 for $TlCu_3S_2$.

indicating that the easiest way to achieve it is if a **B** slab can transform into an **A** slab. Since **B** has the composition $TlCu_4X_2$ and **A** $TlCu_2X_2$, it was suggested that the **A** slabs in $TlCu_3X_2$ are retained (containing the tetrahedrally coordinating Cu(2)), while 50% of the copper in the **B** slab is removed. The copper atoms in that slab belong to two crystallographic sites, Cu(1) and Cu(3), both with a triangular chalcogenide coordination (Table 1). A natural step would be to remove *all* the copper at *one* of these sites to obtain the correct composition, the next step being a crystal shear process along ⟨010⟩ to form the correct coordination of an **A** slab.

Accordingly, copper deficiency of the mother phase is a prerequisite for the transformation. We thus found it worthwhile to investigate which of the three copper sites would be the most "vulnerable" in an oxidative attack.

SYNTHESIS AND NEUTRON DIFFRACTION

$TlCu_3S_2$ was prepared in two steps (3). First Tl_4S_3 was obtained from the elements, thallium being purified beforehand from oxide contamination by melting under vacuum. The binary sulfide was then further reacted with copper and sulfur. The partial degradation of $TlCu_3S_2$ (forming $TlCu_{3-\delta}S_2$ and eventually $TlCu_2S_2$) was accomplished by adding an ammoniacal solution of H_2O_2 dropwise to $TlCu_3S_2$ powder on a glass filter under slow suction by a water-jet pump. The hydrogen peroxide decomposed when in contact with the sulfide, with very reactive oxygen being formed. The ammonia helped in removing the extracted copper into solution by complexing, and the strong color of the ammine complexes served as an indicator for how far the reaction had proceeded.

Neutron diffraction was chosen for monitoring the extraction process instead of X-rays, because the strong X-ray scattering by thallium would dominate the intensity contribution and yield less information on the copper occupancy. Because a whole series of scans was needed, we used a high-flux setup (with lower resolution) devised for studies of amorphous materials rather than the setup normally used for powder diffraction on crystalline substances. The latter would have cost a week's time per scan, whereas with the SLAD (Studsvik Liquids and Amorphous Materials Diffractometer) at Studsvik, Sweden, we could obtain reasonable data after a few hours. This setup has a neutron flux of 10^6 cm^{-2} sec^{-1} at 1.1 Å, monochromatized by Cu(220) and with a step-size of 0.1° yielding an angular resolution of 0.6°.

Nine scans were collected. After each scan the specimen can was left for half an hour to allow the induced radiation to decay; the vanadium can was opened and its contents, about 2 cm^3, were treated for 20 min as described above. Before the treated powder was put back in the can, it was thoroughly washed with water and finally acetone to allow it to dry completely. Inadequate drying showed up immediately as an enhanced background due to absorption by hydrogen.

REFINEMENT OF THE DIFFRACTION DATA

One important feature of the diffractograms was the constant background. This observation immediately suggests that no hydrogen is dissolved, excluding any substitution for copper. The data were analyzed in a multiphase Rietveld program LHPM1 (16). The crystallographic data

TABLE 1
The Copper Sites and Their Sulfur Coordination in $TlCu_3S_2$

Site	Atomic coordinates			CN	Cu–S distances:	(Average)
	x	*y*	*z*			
Cu(1)	0.5933	0	0.6474	3	2.28, 2 × 2.355	2.33
Cu(2)	0.6878	0	0.4290	4	2.23, 2.36, 2 × 2.76	2.53
Cu(3)	0.0571	0	0.3947	3	2 × 2.311, 2.368	2.33

Note. Distances in Ångstrom units. Data were taken from Ref. 17.

as to the positional parameters for $TlCu_3S_2$ were taken from the work of Klepp and Yvon (17), while the cell parameters were independently determined for each extraction by taking a small sample for an X-ray Guinier–Hägg camera using silicon as an internal calibration standard. The refined cell parameters from the neutron data deviated from these owing to a little uncertainty in the neutron wavelength. Because that cannot be refined, it was adjusted in such a way that the refinement of the cell parameters yielded the same parameters as those from the X-ray determination within the error limits suggested from the least-squares treatment.

It was found that the original sample also contained traces of $TlCu_7S_4$ (18) and TlCuS (19). For the former, positional data of $TlCu_7Se_4$ (12) were used, while the latter structure had never been determined. Crystal chemical arguments suggested the *antitype* of PbFCl, which eventually gave a reasonable refinement result. In the extracted samples, $TlCu_2S_2$ clearly dominated over $TlCu_7S_4$, which then was neglected because the program was not able to handle more than three different phases. For $TlCu_2S_2$ the z parameter of $TlCo_2S_2$ (20) was used as starting input.

BAND STRUCTURE CALCULATIONS

The three-dimensional quantum mechanical computations on $TlCu_3S_2$ were based on the original crystallographic parameters by Klepp and Yvon (17). For reasons of computational speed the monoclinic cell ($C2/m$) was first transformed to the fully equivalent smaller triclinic cell ($P\bar{1}$) with $a = 8.298$ Å, $b = 7.566$ Å, $c = 3.863$ Å, $\alpha = 75.209°$, $\beta = 90°$, $\gamma = 69.034°$, and $Z = 2$ (12 atoms). The one-electron Hamiltonian used was that of extended Hückel theory (21, 22), whereas off-site Hamiltonian matrix elements were evaluated according to the weighted Wolfsberg–Helmholz formula (23), minimizing counterintuitive orbital mixing.

The minimal orbital basis set was composed of Slater orbitals that had been fitted to numerical Herman–Skillman functions (24). On-site Hamiltonian matrix elements were approximated by atomic orbital energies from numerical Hartree–Fock calculations (25). In detail, the exchange integrals (ζ orbital exponents in parentheses) were Tl 6s, −9.827 eV (2.303); Tl 6p, −5.235 eV (1.597); S 3s, −24.019 eV (2.020); S 3p, −11.601 eV (1.689); Cu 4s, −6.490 eV (1.444); Cu 4p, −3.359 eV (1.027). For obtaining greater accuracy, the Cu 3d atomic wavefunction (average orbital energy −13.367 eV) was approximated by a double-zeta function with exponents $\zeta_1 = 6.676$, $\zeta_2 = 2.768$ and weighting coefficients $c_1 = 0.487$, $c_2 = 0.657$. The eigenvalue problem was solved in reciprocal space at 64 k-points within the irreducible wedge of the Brillouin zone.

RESULTS AND DISCUSSION

Some results from the structure refinements are shown in Table 2. New structural data were assessed for TlCuS and $TlCu_2S_2$.

A first hint concerning the chemical bonding in the $TlCu_3S_2$ structure arose from the quantum mechanical charges calculated for the atoms. They are +0.478 for Tl, +0.468 for Cu(1), +0.534 for Cu(2), +0.566 for Cu(3), and −1.023 as an average for S(1) and S(2), which are identical within 1.5%. These strongly reduced charges (compared to formal oxidation states) show that much covalency is incorporated and that the great similarity in the crystal chemistry (coordination) of the Cu(1) and Cu(3) atoms is actually not retained in their electronic behavior, possibly because of the difference in second-nearest-neighbor interactions.

A very similar picture emerges from an analysis of the bonding interaction between the metal atoms and the S atoms, here expressed by the numerical value of the integrated overlap population, averaged over the shortest bonds of the couples Tl–S (seven bonds), Cu(1)–S (three bonds), Cu(2)–S (four bonds), and Cu(3)–S (three bonds). These values are 0.055 (Tl–S), 0.318 (Cu(1)–S), 0.207 (Cu(2)–S), and 0.285 (Cu(3)–S). Generally, they scale very nicely with the average bond length. Most important, however, is the fact that Cu(1) and Cu(3), although having an identical average Cu–S bond length of 2.33 Å and similar coordination geometry (Table 1), are truly different species; the Cu(3) atom is less strongly bonded than the Cu(1) atom to the S matrix.

TABLE 2
Some Relevant Parameters from Two Neutron Diffraction Refinements

Run 1 (unextracted)	
R_P	6.4%
R_{wP}	7.9%
$R_I(TlCu_3S_2)$	4.1% (213 refl.)
R_I(TlCuS)	4.1% (45 refl.)
$R_I(TlCu_7S_4)$	3.0% (95 refl.)[a]
Run 8 (extracted)	
R_P	4.8%
R_{wP}	6.2%
$R_I(TlCu_3S_2)$	2.1% (213 refl.)
R_I(TlCuS)	1.8% (45 refl.)[b]
$R_I(TlCu_2S_2)$	1.9% (38 refl.)[c]

[a] Only scale factor refined.

[b] Refined in space-group $P4/nmm$ (anti-PbFCl type), obtaining on site 2c the z parameters 0.74(2) and 0.23(4) for, respectively, Tl and S (with Cu on site 2a).

[c] Refined in space-group $I4/mmm$ ($ThCr_2Si_2$ type), obtaining on site S 4e the z parameter 0.350(3).

Indeed, the refinements of the neutron diffraction experiment showed clearly that the occupancy of only Cu(3) is affected. On consecutive copper extractions its value decreased from $\frac{1}{2}$ to 0.460(8), while the other sites were not significantly different from full occupancy. No trends in positions were noted.

Insight into the reason for this experimental result came from examining the plots of energy-resolved crystal orbital overlap populations (COOP) (26) for the four principally different metal–sulfur interactions, depicted in Figs. 2a–2d. Within these diagrams, spikes on the left (negative scale) stand for antibonding interactions between atoms, whereas spikes on the right (positive scale) show bonding interactions. The broken line stands for the Fermi energy (at $T = 0$ K) which is (roughly speaking) equivalent to the highest filled molecular orbital (HOMO) of a molecule.

The following argument is based on zeroth order perturbation theory reasoning, it assumes that the crystal structure is "frozen" when partial electron density is extracted from it. This physical model for the first step of the oxidation process neglects any lattice relaxation and provides information of limited accuracy (up to second order in

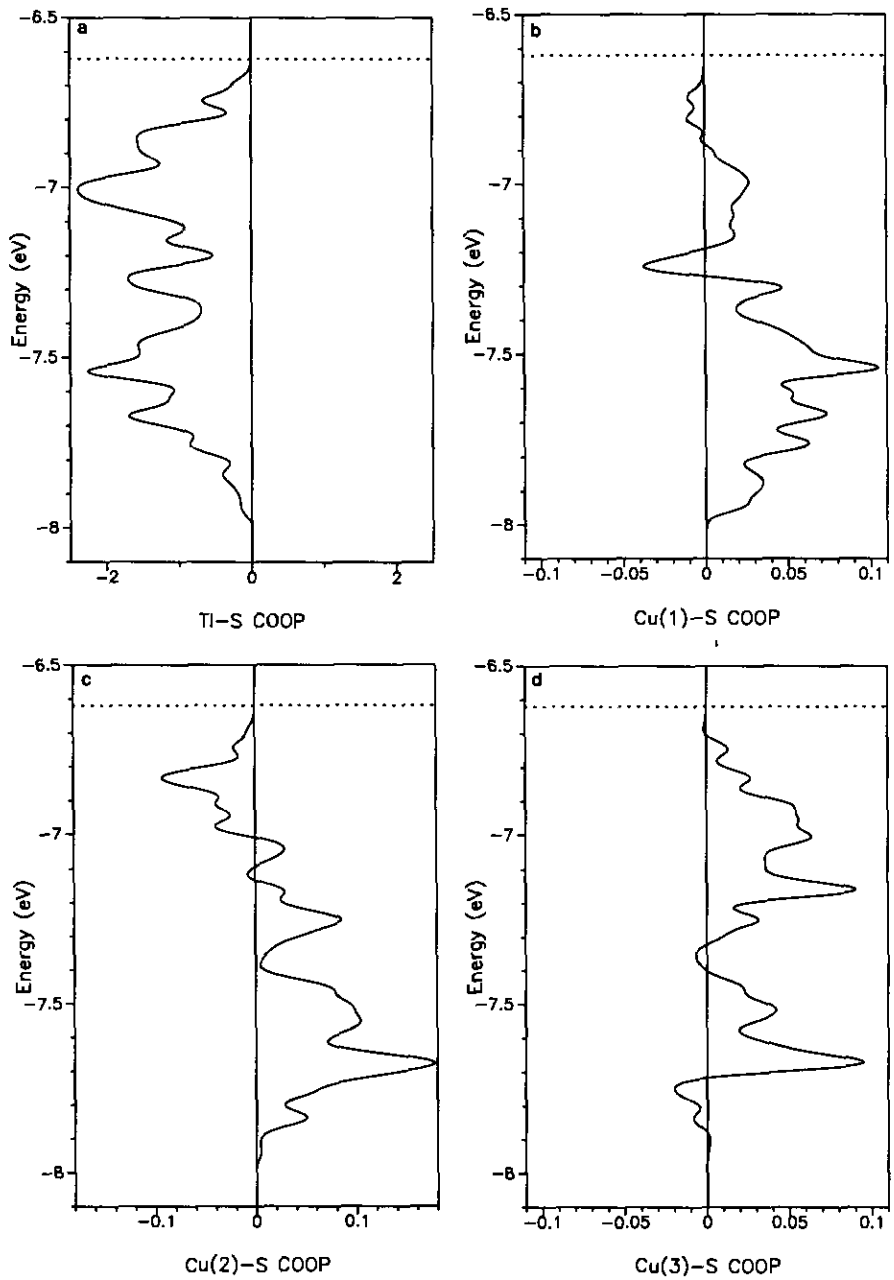

FIG. 2. COOP curves for the various *Me*–S interactions in $TlCu_3S_2$: (a) Tl–S, (b) Cu(1)–S, (c) Cu(2)–S and (d) Cu(3)–S. See text for details.

energy, for example). As we will show in the sequel, however, this approximation is precise enough to yield semiquantitative signposts for the direction in which the oxidation proceeds.

The Tl–S COOP (Fig. 2a) shows that the compound's tendency to be easily oxidized is mainly due to the strongly antibonding Tl–S interactions at the frontier electron bands. Oxidizing the phase will move the Fermi level downward within a frozen-band model, depopulating these antibonding Tl–S levels, i.e., strengthening the Tl–S bonds. Oxidation is thus favored by the Tl–S interaction.

The Cu(1)–S bonds (Fig. 2b) will be virtually unaffected by an oxidation down to a hypothetical Fermi level of about -7 eV since depopulation of antibonding and bonding levels is similar in magnitude. In other words, the Cu(1)–S bonds will remain inert in the course of a beginning oxidation.

In the case of the Cu(2)–S bonds (Fig. 2c), the situation resembles the Tl–S scenario shown before. A slight oxidation will remove electrons from Cu(2)–S levels which are antibonding in character, and the Cu(2)–S bonds will be strengthened slightly. According to the proposed transformation model (2), this Cu atom should survive from $TlCu_3S_2$ on forming the new structure, and this calculation shows that it is the only Cu atom which is stabilized upon oxidation.

Finally we come to Cu(3) and its bonds to sulfur neighbors. The COOP plot (Fig. 2d) shows that only here can one find interactions that are destabilized upon oxidation (depopulating bonding levels), making Cu(3) less strongly bonded within the S matrix. Considering that Cu(3) is already in the unaffected material more weakly bonded than Cu(1), according to the above-mentioned integrated numerical overlap populations, this analysis of the COOP plot gives strong evidence that, among the three different Cu sites inside the structure, Cu(3) is the atom that is "stricken the hardest" by an incoming oxidant, in fact so much so that it must leave the structure, as has been experimentally corroborated by the neutron diffraction refinement.

In addition, one may finally consider that energetic differences play a significant role in the removal of copper from different sites. In other words, one would then neglect the bonding interactions and find the kind of Cu atom that behaves least disruptively with respect to structural change. We have studied this by using a theoretical framework concerning atomic reactivity in solids (27). From net atomic increments of reactivity (excluding bonding interactions) and with respect to the crystal's absolute electronic hardness, the removal of Cu(3) would be favored by more than 0.05 eV compared to the removal of Cu(1). On the other hand, the loss of Cu(1) is favored by about 0.03 eV compared with the loss of Cu(2). Thus, both bonding strength considerations and theoretical investigations concerning disruption upon loss of different copper atoms point in the same direction.

The cell parameters of $TlCu_3S_2$ are sensitive indicators of stoichiometry, and they were found to differ somewhat from the data originally given for stoichiometric material (17). The following parameters were found: a = 14.6116(4) Å, b = 3.8826(2) Å, c = 8.2872(6) Å, β = 111.859(4)°. Extracted material ($TlCu_{2.9}S_2$) gave a = 14.613(2) Å, b = 3.8353(6) Å, c = 8.290(1) Å, β = 111.54(1)°. As has been found for other phases in the Tl–Cu–S system (and Tl–Cu–Se), the short axis becomes still shorter when the phase becomes copper-deficient. The effect has been attributed to the introduction of valence-band holes which, owing to their creation at the top of the band, introduce an effective S–S attraction. Our calculations show that the top of the valence band of $TlCu_3S_2$ indeed corresponds to sulfur p states, most strongly mixing with Tl s levels and in the second place with Cu s–d hybrids. The S–S contraction will occur along the direction that can most efficiently delocalize the holes. In $TlCu_3S_2$ this corresponds to the b axis and in $TlCu_2S_2$ to the a axis. The opposite effect that occurs when the holes are filled was most strikingly illustrated for the solid solutions $TlCu_{2-x}Me_xSe_2$ (Me = Fe, Mn) (10).

CONCLUSIONS

Experimentation and calculations give a consistent picture of which copper atoms are the most vulnerable to an oxidative attack (chemical or electrochemical) on $TlCu_3S_2$. However, although theory and experiment are in agreement regarding the *extraction mechanism*, no full proof of the exact details of the *phase transformation* has been obtained. These data do support the previous model (2) that has otherwise gained some credence from electrochemical measurements and optical microscopy (4, 5).

The agreement opens perspectives for performing theoretical studies on other thallium copper chalcogenide phases as well. For instance, in the $NH_4Cu_7S_4$ type, represented by $TlCu_7S_4$ and $TlCu_7Se_4$, one of the copper sites is even for stoichiometric material filled only to 75% (for charge reasons), compared with the fully occupied $BaCu_8P_4$ (28). Copper extraction in $TlCu_7S_4$ occurs on the site where sulfur is tetrahedrally coordinated (compared with the site Cu(2) in $TlCu_3S_2$) according to experimental evidence (29). Calculations might support these findings. Still more important contributions would be obtained from calculations on $TlCu_5Se_3$ (11), which, on extraction, transforms to a new (orthorhombic) modification of $TlCu_4Se_3$ (1, 2). This structure is not known. Similarly, determining which copper positions of $TlCu_5Se_3$ have the weakest Cu–Se bonding might provide a clue to the mechanism of that transformation and give hints to the structure solution (powder data only accessible).

ACKNOWLEDGMENTS

Financial support was granted by the Swedish Natural Science Research Council (NFR). R. D. expresses his gratitude to Professor Arndt Simon (Stuttgart) for supporting his research activities. Neutron data were collected through the aid of Mr. A. Wannberg and Dr. R. Delaplane.

REFERENCES

1. R. Berger, *J. Solid State Chem.* **70,** 65 (1987).
2. R. Berger, *Chem. Scr.* **28,** 41 (1988).
3. R. Berger, *J. Less-Common Met.* **147,** 141 (1989).
4. R. Berger and R. V. Bucur, *Mater. Res. Bull.* **27,** 439 (1992).
5. R. Berger, R. V. Bucur, and L. Norén, *in* "International Symposium on Chimie Douce", Nantes 1993.
6. F. Viola and R. Schöllhorn, *J. Chem. Soc. Chem. Commun.*, 907 (1992).
7. J.-C. Tédénac, G. Brun, and M. Maurin, *Rev. Chim. Minér.* **18,** 69 (1981).
8. R. Berger and C. F. van Bruggen, *J. Less-Common Met.* **99,** 113 (1984).
9. J. C. V. Folmer and F. Jellinek, *J. Less-Common Met.* **76,** 153 (1980).
10. R. Berger and C. F. van Bruggen, *J. Less-Common Met.* **113,** 291 (1985).
11. R. Berger, L. Eriksson, and A. Meerschaut, *J. Solid State Chem.* **87,** 283 (1990).
12. L. Eriksson, P.-E. Werner, R. Berger, and A. Meerschaut, *J. Solid State Chem.* **90,** 61 (1991).
13. L. Karlsson, M. P. Keane, and R. Berger, *J. Less-Common Met.* **166,** 355 (1990).
14. H. Schils and W. Bronger, *Z. Anorg. Allg. Chem.* **456,** 187 (1979).
15. R. Berger and A. Meerschaut, *Z. Kristallogr.* **185,** 467 (1988); *Eur. J. Solid State Inorg. Chem.* **25,** 279 (1988).
16. R. J. Hill and C. J. Howard, Report, M112, Australian Atomic Energy Commission, Lucas Heights Research Laboratories, Sutherland, New South Wales, 1986.
17. K. Klepp and K. Yvon, *Acta Crystallogr. Sect. B* **36,** 2389 (1980).
18. R. A. Berger and R. J. Sobott, *Monatsh. Chem.* **118,** 967 (1987).
19. B. Gardes, G. Brun, A. Raymond, and J.-C. Tédénac, *Mater. Res. Bull.* **14,** 943 (1979).
20. K. Klepp and H. Boller, *Monatsh. Chem.* **109,** 1049 (1978).
21. R. Hoffmann, *J. Chem. Phys.* **39,** 1397 (1963).
22. R. Hoffmann, "Solids and Surfaces: A Chemist's View of Bonding in Extended Structures", VCH, Weinheim New York, 1988.
23. J. H. Ammeter, H.-B. Bürgi, J. C. Thibeault, and R. Hoffmann, *J. Am. Chem. Soc.* **100,** 3686 (1978).
24. N. J. Fitzpatrick and G. H. Murphy, *Inorg. Chim. Acta* **87,** 41 (1984); *Ibid* **111,** 139 (1986).
25. J. P. Desclaux, *At. Data Nucl. Data Tables* **12,** 3110 (1973).
26. T. Hughbanks and R. Hoffmann, *J. Am. Chem. Soc.* **105,** 3528 (1983).
27. R. Dronskowski, *J. Am. Chem. Soc.* **114,** 7230 (1992).
28. I. Pilchowski, A. Mewis, M. Wenzel, and R. Gruehn, *Z. Anorg. Allg. Chem.* **588,** 109 (1990).
29. R. Berger and L. Norén, unpublished.